Magnetoelectric coupling in the honeycomb antiferromagnet $Co_4Nb_2O_9$

N. D. Khanh,[1,2] N. Abe,[2] H. Sagayama,[3] A. Nakao,[4] T. Hanashima,[4] R. Kiyanagi,[5] Y. Tokunaga,[2] and T. Arima[2]

[1]*Department of Physics, Tohoku University, Sendai 980-8578, Japan*

[2]*Department of Advanced Materials Science, University of Tokyo, Kashiwa 277-8561, Japan*

[3]*Institute of Materials Structure Science, High Energy Accelerator Research Organization, Tsukuba, Ibaraki 305-0801, Japan*

[4]*Research Center for Neutron Science and Technology, CROSS, Tokai, Ibaraki 319-1106, Japan*

[5]*J-PARC Center, Japan Atomic Energy Agency, Tokai, Ibaraki 319-1195, Japan*

(Received 2 June 2015; revised manuscript received 8 January 2016; published 8 February 2016)

The magnetic structure and magnetoelectric effect have been investigated for single crystals of the antiferromagnet $Co_4Nb_2O_9$. Single-crystal neutron diffraction and magnetic susceptibility measurement have revealed that the magnetic structure is different from a collinear arrangement with spin parallel to the trigonal axis as proposed previously. Co^{2+} magnetic moments are found to be almost lying in the basal plane, which lowers the magnetic symmetry to $C2/c'$ with the propagation vector $\boldsymbol{k} = 0$. Associated with the magnetic phase transition, a sharp anomaly in the dielectric constant and displacement current indicate the appearance of the magnetoelectric below Néel temperature T_N with a large coupling constant up to 30 ps/m. The existence of off-diagonal components in a magnetoelectric tensor indicate the formation of ferrotoroidic order in $Co_4Nb_2O_9$. Such a magnetoelectric effect can be ascribed to the reduction of symmetry caused by simple antiferromagnetic order in a honeycomb network.

DOI: 10.1103/PhysRevB.93.075117

Electric field control of magnetic properties of matter is one of the most interesting topics in solid state physics and electronics, toward the innovation of electronic devices [1]. To manipulate over magnetism by an electric field, approaching via magnetoelectric (ME) coupling can be considered as one of the most direct and effective methods. Discovered in the 1960s in Cr_2O_3 [2,3], the ME effect has gained huge attention due to the intriguing fundamental physics as well as the promising possibility to apply it in multifunctional electronic devices. This effect occurs in the system lacking of both time reversal and inversion symmetries simultaneously. As a consequence, the electric polarization (magnetization) could be manipulated by the magnetic field (electric field) [4]. However, due to the strict constraint of symmetry, a limited number of materials that exhibit strong magnetoelectric coupling were found. Recent successful observations of large ME coupling in $TbMnO_3$ [5] and $TbMn_2O_5$ [6] have strongly revived the interest in this topic [7,8]. To date, ME materials are considered as a platform to investigate several novel concepts, including the magnetoelectric monopole [9] or the toroidal moment [10]. Toward the discovery of new phenomena and novel physical mechanisms originating from magnetoelectricity, looking for materials exhibiting stronger magnetoelectric coupling becomes important.

In this work, we present an investigation relating to the ME response in single crystals of cobalt niobate $Co_4Nb_2O_9$. This material belongs to the system of $A_4B_2O_9$ compounds (A = Co, Fe, Mn, and B = Nb, Ta), which were first synthesized and investigated by Bertaut *et al*. [11]. $Co_4Nb_2O_9$ crystallizes in a layered structure belonging to a centrosymmetric trigonal space group $P\bar{3}c1$ (No. 165) with lattice parameters a = 5.177 and c = 14.168 Å. Co^{2+} ions occupy two inequivalent positions, noted as Co(1) and Co(2) with site symmetry 3. Both of Co^{2+} sites are located at the centers of distorted octahedra made of oxygen atoms. As presented in Fig. 1(b), the crystal structure of $Co_4Nb_2O_9$ can be viewed as alternating honeycomb layers consisting of hexagonal rings of $Co(2)O_6$ octahedra stacked between zigzag corner-shared $Co(1)O_6$ octahedra rings. Via powder neutron diffraction, Bertaut and co-workers reported that Co^{2+} magnetic moments order antiferromagnetically parallel to the trigonal axis below T_N = 27.4 K, resulting in the magnetic space group $P\bar{3}'c'1$ (point group $\bar{3}'m'$) with identical magnetic and crystallographic unit cells [11]. As a consequence, a linear ME effect is expected. In fact, the ME effect in $Co_4Nb_2O_9$ was first reported by Fischer *et al*. using a powder sample [12] and reinvestigated recently in polycrystals by Fang *et al*. [13], which revealed a large coupling constant of 18.4 ps/m. In addition to the electric polarization induced by a magnetic field, they found out that $Co_4Nb_2O_9$ also exhibits a large modification of magnetization by an electric field in an antiferromagnetic phase [13]. Motivated by these facts, we performed an investigation using single crystals of $Co_4Nb_2O_9$ necessary to elucidate intriguing ME properties in this material.

We report in this paper an investigation of (i) magnetic structure and (ii) ME coupling using $Co_4Nb_2O_9$ single crystals. In contrast to the previous study [11], our results suggest that the magnetic moment should be aligned almost within the trigonal basal plane, instead of parallel to [001] axis. More intriguingly, a detailed measurement of the ME effect unveils a larger coupling constant compared to previous works, as well as an interesting ME tensor all of whose components are nonvanished, which is found to be related closely to the magnetic symmetry of the system.

Single crystals of $Co_4Nb_2O_9$ were grown by a floating zone method. Stoichiometric amounts of Co_3O_4 and Nb_2O_5 were ground with a molar ratio of 4 : 3 in an agator mortar, compressed into a rod under hydrostatic pressure, and sintered in air at 1100 °C for 48 h. This process was repeated once more to improve the sample quality. The feed rod was zone melted in air and turned into crystal boules. Obtained crystals were characterized by powder x-ray diffraction and the crystal

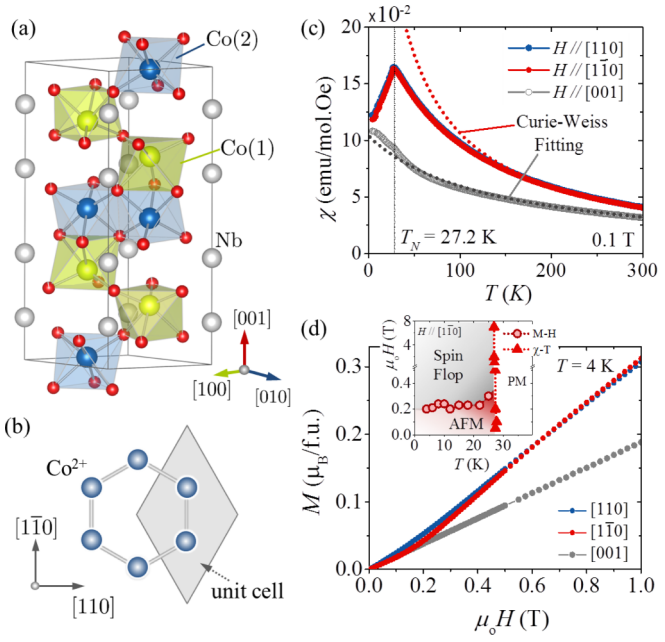

FIG. 1. (a) Crystal structure of $Co_4Nb_2O_9$ and (b) its projection along the trigonal axis. (c) Temperature dependence of magnetic susceptibility in magnetic field 0.1 T along [110],[1$\bar{1}$0], and [001]. The dotted lines exhibit the Curie-Weiss fittings between 200 and 300 K. (d) Magnetization along [110],[1$\bar{1}$0], and [001] at $T = 4.2$ K. The inset shows a magnetic-field–temperature phase diagram in $\boldsymbol{H}\|[1\bar{1}0]$.

orientation was determined by using x-ray Laue photographs. Magnetization was determined using a superconducting quantum interference device (MPMS, Quantum Design). The dielectric constant was measured by using a LCR meter (Agilent E4980A). The electric polarization as a function of temperature and magnetic field was calculated by integrating displacement current with time. To obtain a single-domain state, the sample was cooled in both a magnetic field and a poling electric field. The poling electric field was removed right before measuring the displacement current. Synchrotron x-ray measurements were performed on beam lines BL3A and 8A at the Photon Factory, High Energy Accelerator Research Organization (KEK), Japan. The magnetic structure was determined by neutron diffraction of a single crystal (diameter of 0.5 and length ~1 cm) using a time-of-flight neutron diffractometer BL18 SENJU installed at Materials and Life Science Experimental Facility (MLF), Japan Proton Accelerator Research Complex (J-PARC), Japan. Intensities of 480 reflections (in condition $I > 3\sigma$) were collected at $T = 10$ K. Crystal and magnetic structures with atomic coordination, scale factor, extinction, and volume fraction parameters were refined using JANA 2006 software [14] and visualized by VESTA software [15].

Figure 1(c) shows the temperature dependence of magnetic susceptibility $\chi(T)$ of single crystalline $Co_4Nb_2O_9$ in magnetic field $\mu_0 H = 0.1$ T applied along [110],[1$\bar{1}$0], and [001]. In agreement with previous works [13,16], $\chi(T)$ shows a cusp at $T_N \sim 27.2$ K. However, while $\chi(T)$ along [110] and [1$\bar{1}$0] suddenly decreases below T_N, $\chi(T)$ in $\boldsymbol{H}\|[001]$ gradually increases, which indicates that Co^{2+} magnetic moments should align perpendicularly to the [001] axis. Fitting the linear part of inverse magnetic susceptibility $1/\chi(T)$ between 200 and 300 K to the Curie-Weiss law $\chi(T) = C/(T + \Theta)$, with $C = N_A \mu_{\text{eff}}^2/3k_B$, one can obtain the effective magnetic moment as $\mu_{\text{eff}}^{[110]} \approx \mu_{\text{eff}}^{[1\bar{1}0]} \approx 5.1\mu_B$ and $\mu_{\text{eff}}^{[001]} \approx 5.2\mu_B$. Thereby, the Weiss temperature can be computed as $\Theta_{[110]} \approx \Theta_{[1\bar{1}0]} \approx 24$ and $\Theta_{[001]} \approx 132$ K. Similar to $LiFePO_4$ [17] and $LiCoPO_4$ [18], the magnetic susceptibility exhibits a large difference between in-plane and out-of-plane directions, which implies a remarkable easy-plane type single-ion anisotropy. The ratio between Curie-Weiss Θ and T_N for a magnetic field applied in-plane is almost 1, which indicates that there should not be a significant effect of next nearest neighbor exchange interaction in the honeycomb network. In addition, the effective magnetic moments excess the spin-only value of Co^{2+} ($S = 3/2, \mu_{\text{eff}} = \sqrt{15}\mu_B$) in the high spin configuration, indicating the contribution of the orbital angular momentum to the effective magnetic moment via strong spin-orbit coupling of Co^{2+}. Magnetization $\boldsymbol{M}$ at 4.2 K shown in Fig. 1(d) exhibits linear dependence on the magnetic field in $\boldsymbol{H}\|[001]$ and $\boldsymbol{H}\|[110]$. In contrast, an anomaly standing for a spin-flop phase transition was observed for $\boldsymbol{H}\|[1\bar{1}0]$. This spin flop occurs at $H_c \sim 0.2$ T, which is much smaller than that of polycrystalline sample with $H_c \sim 1.1$ T [13,16]. The results are summarized in a magnetic-field–temperature phase diagram for $\boldsymbol{H}\|[1\bar{1}0]$ presented in the inset in Fig. 1(d). Thus, measurements of the magnetic susceptibility and magnetization performed on single crystalline $Co_4Nb_2O_9$ suggest an in-plane magnetic structure, which is different compared to previous works.

In order to reveal the magnetic structure of $Co_4Nb_2O_9$, a single crystal neutron diffraction was carried out. The crystal structure at 10 K was found to be consistent with synchrotron x-ray data, confirming the absence of a structural phase transition. We observed an increase of (00l) magnetic Bragg reflections with $l = 2n$ below T_N, which can be seen as direct evidence for the in-plane component of magnetic moments. Figure 2(a) displays the integrated intensity of the (002) reflection as a function of temperature that remarkably increases below T_N. Fitting the intensity of the (002) reflection using the power law $m(T)^2 \sim I(T)(1 - T/T_N)^{2\beta}$ yields critical parameter $\beta = 0.2 \pm 0.05$, which indicates the magnetic structure is in the intermediate state between two-dimensional (2D) ($\beta = 0.125$) and three-dimensional (3D) ($\beta = 0.32$) Ising models. This is similar to the situation of the linear ME compound $LiCoPO_4$ [18].

According to symmetry analysis, possible magnetic structures allowed by trigonal symmetry in the crystal structure of $Co_4Nb_2O_9$ can be listed as trigonal ($P\bar{3}c1, P\bar{3}c'1, P\bar{3}'c'1$, and $P\bar{3}'c1$), monoclinic ($C2/c, C2'/c', C2'/c$, and $C2/c'$), and triclinic ($P\bar{1}$ and $P\bar{1}'$). Among them, all the trigonal magnetic space groups indicate magnetic moments parallel to the trigonal axis, which is not consistent with the anisotropy in the magnetic susceptibility. The in-plane magnetic structure, therefore, can be described as a monoclinic or triclinic system. However, monoclinic space groups $C2/c$ and $C2'/c'$ and triclinic $P\bar{1}$ result in a ferromagnetic structure, thus all of them can be excluded. The remaining magnetic space groups that should be considered are $C2/c', C2'/c$, and $P\bar{1}'$.

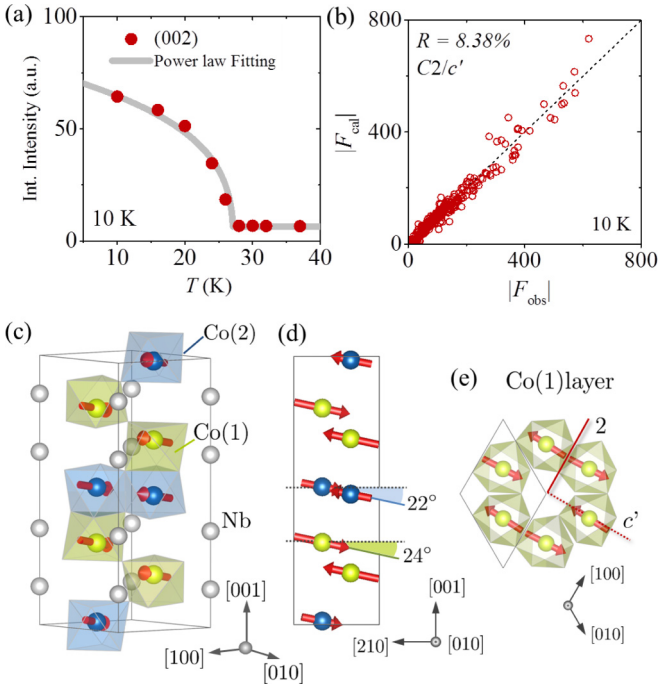

FIG. 2. (a) Integrated intensity of the (002) reflection as a function of temperature. The dark solid line shows the fitting from the power law. (b) Agreement between $|F_{\rm cal}|$ and $|F_{\rm obs}|$ for the magnetic model $C2/c'$. (c) Magnetic structure of $Co_4Nb_2O_9$ with particular views from (d) [010] and (e) [001] axes.

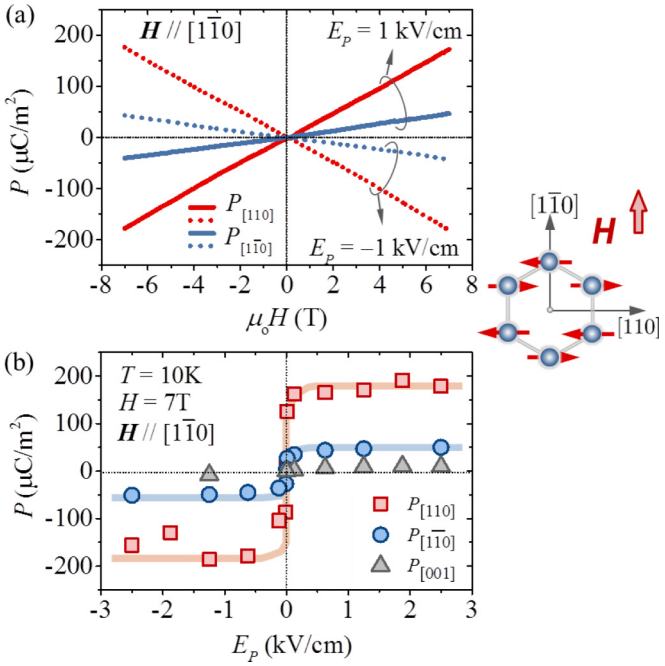

FIG. 3. (a) Magnetic field and (b) poling electric field dependence of $\boldsymbol{P}_{[110]}$, $\boldsymbol{P}_{[1\bar{1}0]}$, and $\boldsymbol{P}_{[001]}$ in magnetic field $\boldsymbol{H}\|[1\bar{1}0]$. Here the solid line in Fig. 3(b) are plotted as guides to the eye.

We obtained the best agreement between experimental data and calculation for magnetic models described by monoclinic magnetic space groups $C2/c'$ and $C2'/c$ (propagation vector $\boldsymbol{k} = 0$). Here 2 (or 2′) and c (or c') are parallel and perpendicular to one of three ⟨110⟩ directions in the trigonal basis. In the latter case, the alignment of magnetic moments parallel to the ⟨010⟩ axis results in larger magnetization along the $[1\bar{1}0]$ direction $\boldsymbol{M}_{[1\bar{1}0]}$ compared to $\boldsymbol{M}_{[110]}$ at low magnetic fields, which disagrees with the observed magnetization clearly showing $\boldsymbol{M}_{[1\bar{1}0]} < \boldsymbol{M}_{[110]}$. Therefore, the model with space group $C2/c'$ is the most favorable to describe the magnetic structure of $Co_4Nb_2O_9$ with residual factor $R = 8.38\%$ ($wR = 15.72\%$) [Fig. 2(b)]. The magnetic structure is illustrated in Figs. 2(c)–2(e). Co^{2+} magnetic moments are aligned perpendicularly to the [110] direction. In a honeycomb layer, neighboring Co^{2+} moments are arranged in opposite directions. The antiferromagnetic honeycomb layers stack along the trigonal axis without changing spin orientation. The magnitudes of magnetic moments of Co^{2+} at distinct crystallographic positions, denoted as Co(1) and Co(2), are $m_{\rm Co(1)} \approx 3.5\mu_B$ and $m_{\rm Co(2)} \approx 2.6\mu_B$, respectively. Both $m_{\rm Co(1)}$ and $m_{\rm Co(2)}$ exhibit a canting angle of around 20° away from the basal plane.

As reported in recent works [13,16], a large ME effect was found in $Co_4Nb_2O_9$ below the Néel temperature. Nevertheless, all of them were obtained from polycrystals and interpreted based on a magnetic structure with Co^{2+} magnetic moments aligning along the trigonal axis. Using single crystalline samples, we present below a detailed investigation of the ME effect of $Co_4Nb_2O_9$ and an explanation based on a different magnetic structure.

Figure 3 displays the dependence of polarizations $\boldsymbol{P}_{[110]}$ and $\boldsymbol{P}_{[1\bar{1}0]}$ on an external magnetic field applied parallel to the $[1\bar{1}0]$ direction. Both of them exhibit a linear increase with the magnetic field up to 7 T applied along the $[1\bar{1}0]$ axis, which confirms the linear ME effect in $Co_4Nb_2O_9$. Magnetic-field induced polarization can be absolutely switched between $+P$ and $-P$ by reversing the poling electric field E_p without causing any adjustment to the magnitude, as demonstrated in Fig. 3(a). Cooling down the sample in $H = +7$ T and $E_p > 0$ results in a positive polarization, while a negative one can be achieved via poling with $H = +7$ T and $E_p < 0$. A large $P_{[110]}$ up to 200 μC/m^2 can be achieved in a magnetic field of 7 T, corresponding to a linear ME coupling constant of ∼30 ps/m. This value is quite large compared to that of other typical linear ME compounds like Cr_2O_3 [3,19], $Ga_{2-x}Fe_xO_3$ [20], $MnTiO_3$ [21], LiMPO$_4$ (M = Mn, Fe, or Co) [18,22], or $NdCrTiO_5$ [23]. Finally, the effect of poling electric field $\boldsymbol{E}_p$ on polarization is summarized in Fig. 3(b). Above 0.5 kV/cm, the magnitude of polarization becomes saturated and independent to $\boldsymbol{E}_p$ even up to 2.5 kV/cm, which implies the stability of ME domains upon the poling process.

A more detailed examination of ME coupling is introduced in Fig. 4. The measurement of polarization as a function of temperature was performed in magnetic field $\boldsymbol{H}$ and poling electric field $\boldsymbol{E}_p$ applied along [110],$[1\bar{1}0]$, and [001] axes, alternatively. The results reveal an intriguing ME tensor with all components nonvanished. Associated with a magnetic phase transition at $T_N = 27$ K, a sharp anomaly in dielectric constant (not shown) and the onset of a displacement current were observed at T_N, which implies the emergence of an

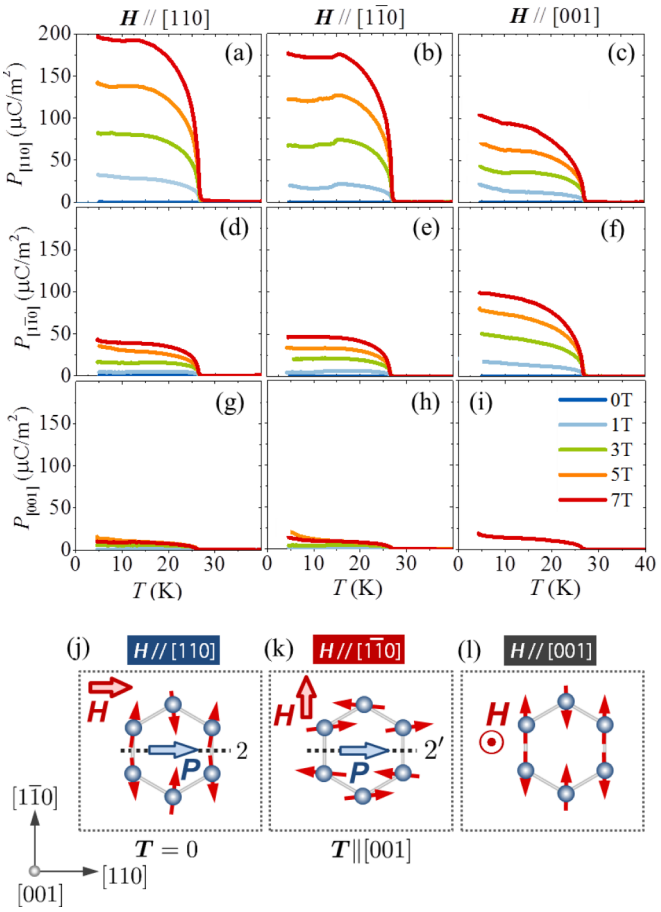

FIG. 4. (a)–(i) Temperature dependence of polarization in the magnetic field and the poling electric field applied along [110],[1$\bar{1}$0], and [001], alternatively. The relationship between external magnetic field $\boldsymbol{H}$ and induced polarization $\boldsymbol{P}$ with magnetic symmetry in (j) $\boldsymbol{H}\|[110]$, (k) $\boldsymbol{H}\|[1\bar{1}0]$, and (l) $\boldsymbol{H}\|[001]$.

electric polarization under the presence of an external magnetic field. Up to $H = 7$ T, a polarization of $\sim$200 μC/m^2 was achieved for $\boldsymbol{P}_{[110]}$ in $\boldsymbol{H}\|[110]$ or $\boldsymbol{H}\|[1\bar{1}0]$. Meanwhile, $\boldsymbol{P}_{[001]}$ posed a small polarization of $\sim$15 μC/m^2 in any direction of the magnetic field. $\boldsymbol{P}_{[110]}$ is almost four times larger than $\boldsymbol{P}_{[1\bar{1}0]}$ in a magnetic field applied in-plane. It should be noted that in all cases, the polarization increases at T_N and reaches a saturation value at low temperature, instead of diminishing to zero. This can be attributed to the fact that the ME effect was observed at a magnetic field much higher than the spin-flop phase transition, where all magnetic moments are aligned almost perpendicularly to the magnetic field. In any case, the polarization exhibits a linear dependence on the magnetic field up to 7 T at 5 K. The existence of several off-diagonal components in the ME tensor may imply the appearance of toroidal moment $\boldsymbol{T} \sim (\boldsymbol{P} \times \boldsymbol{M})$. As described intensively in the literature, the emergence of such a ferrotoroidic state has been considered as the origin of several intriguing effects [10,24], such as a modification of band structure [25,26], nonreciprocal effects [27–30], or other nonlinear optical phenomena [31,32].

Due to the absence of a structural phase transition, the observed ME tensor can be explained in terms of symmetry lowering due to the ordering of the magnetic moment. We next discuss the relationship between the revised magnetic structure with the observed ME effect, as shown schematically in Figs. 4(j)–4(l). Because the measurement of the polarization was carried out at magnetic fields above the spin-flop phase transition (for $\boldsymbol{H}\|[110]$ or $\boldsymbol{H}\|[1\bar{1}0]$ at $\mu_0 H_C \approx$ 0.2 T, a fairly weak magnetic anisotropy may be expected. Therefore, a magnetic field of 7 T of this experiment is considered to be large enough to align the antiferromagnetic component orientated perpendicularly to the direction of the magnetic field. Thus, the ME response is related closely to the magnetic structure at the spin-flop phase as well as the ground state.

In particular, for $\boldsymbol{H}\|[110]$, the two-fold axis $2\|[110]$ can remain unchanged while the glide plane associated time reversal symmetry $c' \perp [110]$ is broken [Fig. 4(j)]. Electric polarization can emerge along the two-fold rotation axis. Meanwhile, the application of $\boldsymbol{H}\|[1\bar{1}0]$ results in $2'\|[110]$ and breaks $c \perp [110]$ [Fig. 4(k)]. Clearly, $\boldsymbol{P}_{[110]}$ is nonzero. Note that in this case, the polarization $\boldsymbol{P}_{[110]}$ was induced transverse to the magnetic field direction $\boldsymbol{H}\|[1\bar{1}0]$. As a consequence, the formation of a ferrotoroidic state where toroidal moments align parallel to the trigonal axis can be expected. This may lead to the observation of, for instance, directional dichroism for light propagating in the opposite ways along the [001] axis. Briefly speaking, an application of a magnetic field in the basal plane parallel to [110] or [1$\bar{1}$0] always induces $\boldsymbol{P}_{[110]}$, which is the largest polarization that can be observed in the ME tensor. In the case $\boldsymbol{H}\|[001]$ [Fig. 4(l)], the application of the magnetic field does not cause a spin-flop transition which makes $c' \perp [010]$ unchanged, while a two-fold rotation no longer remains. Thereby, the polarization perpendicular to [010], $\boldsymbol{P}_{[1\bar{1}0]}$ and $\boldsymbol{P}_{[001]}$, can appear.

As discussed above, the ME tensor related to magnetic structure $C2/c'$ itself does not predict the appearance of $\boldsymbol{P}_{[1\bar{1}0]}$. One possibility is that the polarization $\boldsymbol{P}_{[1\bar{1}0]}$ in $\boldsymbol{H}\|[110]$ or $\boldsymbol{H}\|[1\bar{1}0]$, and $\boldsymbol{P}_{[110]}$ in $\boldsymbol{H}\|[001]$ can appear in different magnetic domains, which may grow via a poling process in both a magnetic field and an electric field. For the poling magnetic field within the basal plane, a fairly strong electric field in the poling process may create some minor magnetic domains. Antiferromagnetic moments would not be aligned perpendicularly to the direction of the magnetic field, and thereby generate some minor ferroelectric domains corresponding to the existence of $\boldsymbol{P}_{[1\bar{1}0]}$. Therefore, the magnetic structure described by $C2/c'$ symmetry is indeed reasonable to explain the behavior of the magnetic property as well as the ME response in this compound.

Next, we would like to discuss the possible microscopic mechanism of ME coupling. Up to date, the magnetic field induced electric polarization can be understood microscopically under the framework of the three most popular mechanisms: (1) the spin current (or inverse Dzyalonshinskii-Moriya interaction) mechanism [33], (2) the magnetostriction mechanism [34], and (3) the spin dependent metal-ligand hybridization mechanism [35,36]. Among them, the Dzyaloshinskii-Moriya mechanism [33] induces electric dipole $\Delta \boldsymbol{P} \propto \boldsymbol{e}_{ij} \times (\boldsymbol{S}_i \times \boldsymbol{S}_j)$ at the bond between sites i and j. Here $\boldsymbol{S}_i, \boldsymbol{S}_j$ denote spin moments at neighboring sites, while $\boldsymbol{e}_{ij}$ is the unit vector.

For a magnetic field applied in-plane, $(\boldsymbol{S}_i \times \boldsymbol{S}_j)$ should orient along the trigonal axis. The summation of the three unit vectors $\boldsymbol{e}_{ij}$ representing Co-Co bonds in a honeycomb network also directs parallel to the trigonal axis. Thus, we cannot expect any net polarization from this mechanism. In addition, $Co_4Nb_2O_9$ crystallizes in a centrosymmetric space group $P\bar{3}c1$, which does not allow a piezoelectric response. The crystal structure is confirmed to remain down to a low temperature of 10 K. A macroscopic electric polarization can not be induced upon a lattice deformation. Therefore, we also exclude the possibility that the observed ME effect could be ascribed to the modification of a local electric dipole moment by the scalar product of neighboring magnetic moments as $\Delta \boldsymbol{P} \propto (\boldsymbol{S}_i \cdot \boldsymbol{S}_j)$, referred to the magnetostriction mechanism. Finally, according to the metal-ligand hybridization model, induced polarization is proportional to $\Delta \boldsymbol{P} \propto (\boldsymbol{S}_i \cdot \boldsymbol{e}_{ij})^2 \boldsymbol{e}_{ij}$, which means that the polarization should be an even function of the magnetic field. However, in our case, the polarization changed sign upon the sweeping of the magnetic field. Therefore, ME coupling in this compound also can not be explained reasonably by the metal-ligand hybridization mechanism.

Keeping in mind that orbital angular momentum in $Co_4Nb_2O_9$ is not quenched completely because of Co^{2+} 's strong spin-orbit coupling, orbital moments can contribute to the emergence of linear magnetoelectricity as proposed recently [37]. The effect can be identified via examination of the dependence of the orbital angular momentum on an external applied electric field. Thus, we do not neglect the possibility that the cross correlation between an electric polarization and a magnetic field, as well as the magnetization and the electric field in $Co_4Nb_2O_9$, may partially originate from the orbital moment and this is worth investigating in future study. Therefore, further investigation is motivated to elucidate the microscopic origin of the ME response in $Co_4Nb_2O_9$.

In conclusion, we have investigated the magnetic structure and ME response in single crystalline $Co_4Nb_2O_9$. The results suggest that $Co_4Nb_2O_9$ exhibits an in-plane antiferromagnetic order described by the magnetic space group $C2/c'$ (propagation vector $\boldsymbol{k} = 0$). The reduction of symmetry due to magnetic order leads to the emergence of the ME response. Off-diagonal components in the ME tensor indicate the formation of a ferrotoroidic order, which may give rise to intriguing phenomena related to the coupling between magnetic order and ferroelectricity.

We acknowledge fruitful discussions with Y. Nii, T. Nakajima, and K. Matsuura and would like to thank N. Netsu for assistance in the experiments. This work was supported by a Grant-In-Aid for Scientific Research (No. 24244045) from Japan Society for the Promotion of Science. The study of the magnetic property and Laue photograph were carried out at the Institute for Solid State Physics, University of Tokyo, Japan. The ME response was partly investigated at the High Field Laboratory for Superconducting Materials, Institute for Materials Research, Tohoku University, Japan.

[1] F. Matsukura, Y. Tokura, and H. Ohno, Nat. Nanotech. **4**, 158 (2009).
[2] I. E. Dzyaloshinskii, Sov. Phys. JETP **10**, 628 (1960).
[3] D. N. Astrov, Sov. Phys. JETP **11**, 708 (1960).
[4] M. Fiebig, J. Phys. D: Appl. Phys. **38**, R123 (2005).
[5] T. Kimura, T. Goto, H. Shintani, K. Ishizaka, T. Arima, and Y. Tokura, Nature (London) **426**, 55 (2003).
[6] N. Hur, S. Park, P. A. Sharma, J. S. Ahn, S. Guha, and S. W. Cheong, Nature (London) **429**, 392 (2004).
[7] T. Arima, J. Phys. Soc. Jpn. **80**, 052001 (2011).
[8] Y. Tokura, S. Seki, and N. Nagaosa, Rep. Prog. Phys. **77**, 076501 (2014).
[9] N. A. Spaldin, M. Fechner, E. Bousquet, A. Balatsky, and L. Nordström, Phys. Rev. B **88**, 094429 (2013).
[10] N. A. Spaldin, M. Fiebig, and M. Mostovoy, J. Phys.: Condens. Matter **20**, 434203 (2008).
[11] E. F. Bertaut, L. Corliss, F. Forrat, R. Aleonard, and R. Pauthenet, J. Phys. Chem. Solids **21**, 234 (1961).
[12] E. Fischer, G. Gorodetsky, and R. M. Hornreich, Solid State Commun. **10**, 1127 (1972).
[13] Y. Fang, Y. Q. Song, W. P. Zhou, R. Zhao, R. J. Tang, H. Yang, L. Y. Lv, S. G. Yang, D. H. Wang, and Y. W. Du, Sci. Rep. **4**, 3860 (2014).
[14] V. Petricek, M. Dusek, and L. Palatinus, Z. Kristallogr. **229**, 345 (2014).
[15] K. Momma and F. Izumi, J. Appl. Crystallogr. **44**, 1272 (2011).
[16] T. Kolodiazhnyi, H. Sakurai, and N. Vittayakorn, Appl. Phys. Lett. **99**, 132906 (2011).
[17] G. Liang, K. Park, J. Li, R. E. Benson, D. Vaknin, J. T. Markert, and M. C. Croft, Phys. Rev. B **77**, 064414 (2008).
[18] D. Vaknin, J. L. Zarestky, L. L. Miller, J.-P. Rivera, and H. Schmid, Phys. Rev. B **65**, 224414 (2002).
[19] A. Iyama and T. Kimura, Phys. Rev. B **87**, 180408(R) (2013).
[20] T. Arima, D. Higashiyama, Y. Kaneko, J. P. He, T. Goto, S. Miyasaka, T. Kimura, K. Oikawa, T. Kamiyama, R. Kumai, and Y. Tokura, Phys. Rev. B **70**, 064426 (2004).
[21] N. Mufti, G. R. Blake, M. Mostovoy, S. Riyadi, A. A. Nugroho, and T. T. M. Palstra, Phys. Rev. B **83**, 104416 (2011).
[22] M. Mercier and J. Gareyte, Solid State Commun. **5**, 139 (1967).
[23] J. Hwang, E. S. Choi, H. D. Zhou, J. Lu, and P. Schlottmann, Phys. Rev. B **85**, 024415 (2012).
[24] T. Arima, J. Phys.: Condens. Matter **20**, 434211 (2008).
[25] S. Hayami, H. Kusunose, and Y. Motome, Phys. Rev. B **90**, 024432(R) (2014).
[26] S. Hayami, H. Kusunose, and Y. Motome, Phys. Rev. B **90**, 081115(R) (2014).
[27] K. Sawada and N. Nagaosa, Phys. Rev. Lett. **95**, 237402 (2005).
[28] D. Szaller, S. Bordacs, and I. Kezsmarki, Phys. Rev. B **87**, 014421 (2013).

[29] N. D. Khanh, N. Abe, K. Kubo, M. Akaki, M. Tokunaga, T. Sasaki, and T. Arima, Phys. Rev. B **87**, 184416 (2013).
[30] S. Toyoda, N. Abe, S. Kimura, Y. H. Matsuda, T. Nomura, A. Ikeda, S. Takeyama, and T. Arima, Phys. Rev. Lett. **115**, 267207 (2015).
[31] B. B. Van Aken, J.-P. Rivera, H. Schmid, and M. Fiebig, Nature (London) **449**, 702 (2007).
[32] A. S. Zimmermann, D. Meier, and M. Fiebig, Nat. Commun. **5**, 4796 (2014).
[33] H. Katsura, N. Nagaosa, and A. V. Balatsky, Phys. Rev. Lett. **95**, 057205 (2005).
[34] I. A. Sergienko and E. Dagotto, Phys. Rev. B **73**, 094434 (2006).
[35] T. Arima, J. Phys. Soc. Jpn. **76**, 073702 (2007).
[36] C. Jia, S. Onoda, N. Nagaosa, and J. H. Han, Phys. Rev. B **76**, 144424 (2007).
[37] A. Scaramucci, E. Bousquet, M. Fechner, M. Mostovoy, and N. A. Spaldin, Phys. Rev. Lett. **109**, 197203 (2012).